Ionic Conductivity of $Li_2B_4O_7$

Mazharul M. Islam,[†] Thomas Bredow,*[,‡] and Christian Minot[§]

Applied Centre for Structural and Synchrotron Studies, University of South Australia, Mawson Lakes Campus, Mawson Lakes, Adelaide, South Australia 5095, Australia, Institut für Physikalische und Theoretische Chemie, Universität Bonn, Wegelerstr. 12, 53115 Bonn, Germany, and Laboratoire de Chimie Théorique, UMR 7616 CNRS, Université P. et M. Curie, Case 137, Tour 23-22, 4 Place Jussieu, Paris 75252 Cédex 05, France

Received: March 22, 2006; In Final Form: July 3, 2006

The formation and mobility of Li point defects in $Li_2B_4O_7$ are investigated theoretically with periodic quantum chemical calculations. Calculated defect formation energies obtained with a density functional theory/Hartree−Fock hybrid method and with the Perdew−Wang density functional method are compared. The basis set effect is investigated by comparison of results obtained with atom-centered basis functions and plane waves. With both methods only a moderate relaxation is observed for the atoms surrounding the Li defect position. The defect-induced change of electronic properties is investigated by calculating the density of states for the stoichiometric and defective supercells. The activation energy for the movement of a Li^+ ion along the (001) direction is calculated. It is observed that Li^+ ion migrates through a one-dimensional channel formed by the five-vertex lithium−oxygen (LiO_5) polyhedra. The calculated activation energies are in excellent accord with experiment.

1. Introduction

Crystalline lithium tetraborate (LTB) $Li_2B_4O_7$ is of considerable interest due to its practical applications. LTB has important physical properties,[1] such as a high coefficient of electrochemical coupling, low velocity of propagation of surface acoustic waves, zero thermal expansion coefficient, high mechanical strength, and low electrical conductivity at room temperature. It is used for laser radiation converters,[2] as substrate for thermostable surface[3−5] and bulk[6] acoustic wave-based devices, as piezoelectric nonlinear optical device for second harmonic generation,[7−9] in electroacoustic devices,[10−12] as a pyroelectric sensor,[12,13] and in thermoluminescent dosimetry of X-ray, γ-ray, and neutron radiation.[14−16]

$Li_2B_4O_7$ belongs to space group $I4_1cd$ and has 52 atoms (four formula units) per primitive unit cell.[17−19] The measured lattice parameters are $a = 9.48$ Å and $c = 10.29$ Å. The main structural pattern is a $[B_4O_9]^{6-}$ complex which consists of two planar trigonal (BO_3) and two tetrahedral (BO_4) units. Lithium ions are connected with the anion subsystem electrostatically.[17] The loose connectivity results in the appearance of ionic conductivity and superionic properties.[20] Experimental investigations[21,22] for the temperature dependence of conductivity for LTB single crystals showed that the conductivity along the tetragonal *c* axis is higher by almost 5 orders of magnitude than along the perpendicular direction. In these studies it was established that the conductivity of LTB crystals is purely electronic along the (100) direction and purely ionic (via transport of Li ions) along the (001) direction. Since then, several experimental investigations have been performed to study the ionic conductivity of this system along the (001) direction.[23−28] It was suggested[23] that the conduction of Li^+ ion occurs through a one-dimensional channel in the tetragonal axis. This conductivity channel is formed by triangular faces of the five-vertex oxygen polyhedra around the main lithium position. The ionic conductivity in LTB is attributed to the Li vacancies.[23−25]

Several different values for the activation energy E_A of the ion migration in LTB exist in the literature. They are depending on the preparation method of the samples.[23] Kim et al.[25] measured E_A for the LTB crystals prepared from $Li_2B_4O_7$ powder (LTBp, 0.42 eV) and from $Li_2CO_3-B_2O_3$ mixed powder (LTBm, 0.46 eV).

In the present study, a theoretical investigation of the Li vacancy defect and the migration of a Li^+ ion in LTB is performed using first-principles methods and periodic supercell models. The activation energy is calculated for the Li^+ ion movement from its original position to an adjacent Li vacancy position along the (001) direction.

2. Computational Methods

The investigation of Li vacancy defect properties and migration of Li^+ ion in $Li_2B_4O_7$ was performed with the HF-DFT hybrid method PW1PW and with the density-functional method PW91. In this way the effect of the description of exchange on the calculated properties could be studied. In the PW1PW hybrid method,[29] the exchange functional is a linear combination of the HF expression (20%) and the Perdew−Wang[30,31] exchange functional (80%). Electron correlation is described with the PW91 correlation functional.[30,31] PW1PW is similar to the mPW1PW91 functional proposed by Adamo and Barone[32] but uses the original PW91 exchange functional, rather than the modified form introduced by these workers. The exact-exchange coefficient is also reduced from 25% to 20%. This approach has been applied for calculations of bulk properties of MgO, NiO, CoO,[29] TiO_2,[33] Li_2O,[34] B_2O_3,[35] and $Li_2B_4O_7$[36] and electronic properties of $Li_2O-B_2O_3$ compounds.[37] In these studies, good agreement between calculated and experimental bulk properties was observed for the PW1PW

[†] University of South Australia.
[‡] Universität Bonn.
[§] Université P. et M. Curie.

10.1021/jp061785j CCC: $33.50
Published on Web 08/15/2006

TABLE 1: Comparison of Calculated Lattice Vectors *a* and *c* (Å), Binding Energy per $Li_2B_4O_7$ Unit E_u (eV) and Band Gap E_g (eV) with Experimental Values

properties	PW1PW	PW91-PAW	exptl
a	9.50	9.42	9.48[a]
c	10.32	10.22	10.29[a]
E_u	−79.5	−84.3	−79.4[b]
E_g	9.31	6.18	9.00[c]

[a] Reference 17. [b] Reference 47. [c] Extrapolated from the fundamental absorption energy ref 48.

TABLE 2: Effect of Relaxation on the Formation Energy of a Single Li Vacancy, E_{de}(V) (eV) in $Li_2B_4O_7$

	PW1PW	PW91-PAW
unrelaxed	8.3	7.2
relaxed	7.5	6.8

method. It was observed that PW1PW gives the best reproduction of experimental activation energies (E_A) for the Li^+ ion migration in Li_2O among the considered methods.[34] This DFT approach was used as implemented in the crystalline orbital program CRYSTAL03.[38] In CRYSTAL the Bloch functions are linear combinations of atomic orbitals. The quality of the results is therefore affected by the choice of the atomic basis set. In a previous study,[36] we investigated the effect of basis set on the structural, energetic, and electronic properties of $Li_2B_4O_7$. From our previous experience, we considered the following combination of basis sets: 6-11G[39] for lithium, 6-21G*[40] for boron, and 8-411G*[41] for oxygen. Taking into account that the investigation of defect properties and ion migration should be done with large supercells in order to avoid direct defect−defect interactions, this combination of the basis set is a good compromise between accuracy and computational effort.

The second approach denoted as PW91-PAW is the Perdew−Wang DFT method[30,31] as implemented in the plane wave program VASP.[42−44] In contrast to the LCAO approach which allows the explicit treatment of all electrons, inner electrons are replaced by effective potentials in the plane wave program. On the basis of our previous study of $Li_2B_4O_7$,[36] we used projector augmented wave (PAW) potentials.[45,46] A set of plane waves with an energy cutoff (E_{cut}) 400 eV describes the valence electrons.

3. Results and Discussion

First, we briefly summarize the calculated bulk properties of stoichiometric $Li_2B_4O_7$ as obtained in a previous study,[36] such as structure parameters, binding energy, and band gap. Then we present results on defect properties: the vacancy formation energy, structural changes around the Li vacancy, defect-induced features in the electronic structure, and the Li^+ ion migration.

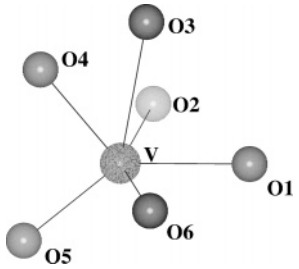

Figure 1. Six nearest oxygen atoms from the Li vacancy (V) in the LTB crystal.

3.1. Bulk Properties of Stoichiometric $Li_2B_4O_7$. A comparison of calculated values for the lattice parameters *a* and *c*, the binding energy per $Li_2B_4O_7$ unit E_u, and the band gap E_g as obtained with PW1PW and PW91-PAW with experimental values is given in Table 1. PW1PW in general better reproduces the experimental bulk properties. With the PW91-PAW approach the lattice parameters and band gap are underestimated, whereas a more negative value for E_u is obtained. This difference will be taken into account in the discussion of the defect properties.

3.2. Cation Vacancy in Lithium Tetraborate. For the simulation of a Li vacancy in LTB, a supercell $Li_{16}B_{32}O_{56}$ was created by applying the transformation matrix **L** (3.1) on the primitive unit cell.

$$\mathbf{L} = \begin{pmatrix} 0 & 1 & 1 \\ 1 & 0 & 1 \\ 1 & 1 & 0 \end{pmatrix} \tag{3.1}$$

This supercell corresponds to the conventional unit cell of $Li_2B_4O_7$ and contains 104 atoms. A full optimization of atomic fractional coordinates was performed taking the optimized lattice parameters (a = 9.50 Å and b = 10.32 Å) from the bulk optimization (Table 1). One neutral Li atom was removed from the cell to create the defective system. This leads to an open-shell electronic structure with one unpaired electron per cell. The calculations were therefore performed using the spin-polarized method. Corresponding defect calculations of a charged Li^+ defect failed due to severe SCF convergence problems. In these calculations a homogeneous background

TABLE 3: Distances *r* (Å) of the nearest Oxygen Atoms from the Li Vacancy (V) and Changes Δ*r* of the Distances (in % of *r*) Due to Relaxation

		PW1PW			PW91-PAW		
distance	vacancy−atom	unrelaxed	relaxed	Δ*r*, %	unrelaxed	relaxed	Δ*r*, %
r_1	V−O1	1.96	2.04	+4.1	1.96	2.03	+3.0
r_2	V−O2	2.00	2.10	+5.0	2.00	2.08	+4.0
r_3	V−O3	2.08	2.13	+2.4	2.07	2.13	+2.9
r_4	V−O4	2.09	2.18	+4.3	2.11	2.15	+1.9
r_5	V−O5	2.73	2.85	+4.4	2.62	2.82	+7.6
r_6	V−O6	2.84	2.85	+0.2	2.63	2.84	+0.4

TABLE 4: Distances *r* (Å) of the nearest Boron and Lithium Atoms from the Li Vacancy (V) and Changes Δ*r* of the Distances (in % of *r*) Due to Relaxation

		PW1PW			PW91-PAW		
distance	vacancy−atom	unrelaxed	relaxed	Δ*r*	unrelaxed	relaxed	Δ*r*
r_1	V−B1	2.66	2.65	−0.4	2.66	2.64	−0.8
r_2	V−B2	2.69	2.69	−0.7	2.68	2.65	−1.1
r_3	V−B3	2.86	2.86	−0.0	2.84	2.83	−0.2
r_4	V−Li	3.06	2.93	−4.2	3.08	2.99	−2.9

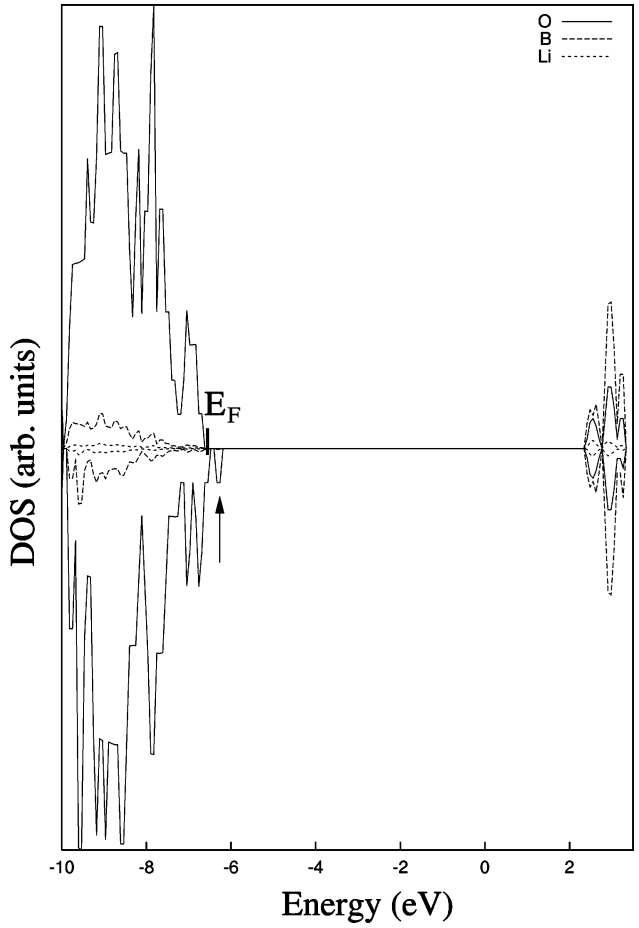

Figure 2. Density of states (DOS) for Li vacancy in $Li_{16}B_{32}O_{56}$ obtained with PW1PW. E_F denotes the Fermi level.

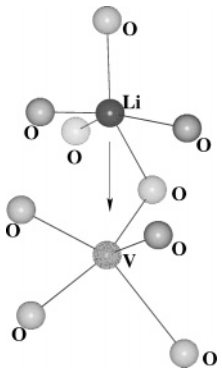

Figure 3. Two nearest oxygen five-vertex polyhedra of lithium and vacancy (V) along the tetragonal axis of the LTB crystal. The light (dark) gray spheres denote oxygen atoms below (above) the Li−V plane.

charge was added to ensure electroneutrality. Therefore in the following we only present results for the neutral Li vacancy. The optimized fractional coordinates of the nondefective supercell were taken as starting structure for the defective system. This artificial "frozen" geometry will be denoted as *unrelaxed* structure in the following. In the next step a full optimization of all remaining atoms of the defective cell was performed without symmetry constraints. The final structure will be referenced as *relaxed*. The energy lowering due to structure optimization will be denoted as relaxation energy E_R. For both geometries the formation energy of a Li vacancy $E_{de}(V)$ is calculated according to the equation

$$E_{de}(V) = E^{SCM}(V) + E(Li) - E^{SCM} \qquad (3.2)$$

Here $E^{SCM}(V)$ and E^{SCM} denote the total energy of the supercell model with and without vacancy, respectively, and $E(Li)$ is the energy of the free Li atom. As described in the previous study on $Li_2B_4O_7$ bulk properties,[36] extended basis sets and cutoff energies were used for the atomic reference calculations. In Table 2, the calculated $E_{de}(V)$ are presented for the relaxed and unrelaxed supercells. To our knowledge there is no previous experimental or theoretical value of the Li vacancy formation energy of LTB. Therefore the calculated $E_{de}(V)$ values obtained with PW1PW and PW91-PAW are compared with each other in the following. Since PW1PW gives the best reproduction of the experimental bulk properties of LTB[36] and of the defect properties of Li_2O,[34] this method is taken as reference. The $E_{de}(V)$ for the fully relaxed system obtained with PW1PW is 7.5 eV. As for Li vacancy defect in Li_2O, the PW91-PAW approach gives a significantly smaller value of $E_{de}(V)$ (6.8 eV) compared to PW1PW. The absolute values for the Li defect formation energy is considerably higher in $Li_2B_4O_7$ than in Li_2O. There we obtained 5.9 eV (PW1PW) and 4.9 eV (PW91-PAW). In part this can be explained by the larger band gap in LTB (9.3 eV, Table 1) compared to Li_2O (8.0 eV, PW1PW[34]). For both systems the top of the valence band is dominated by O 2p levels whereas the lower part of the conduction band consists mainly of Li 2sp orbitals (Li_2O) or Li 2sp and B 2sp orbitals ($Li_2B_4O_7$), respectively.[37] Therefore the reduction of an oxygen atom after removal of a Li atom is energetically less costly in the system with the smaller band gap. For a more quantitative analysis we compared the Mulliken overlap population of Li with its neighbors in $Li_2B_4O_7$ and Li_2O. Surprisingly, the overlap population to the four nearest oxygen neighbors is larger in Li_2O (0.043) than in $Li_2B_4O_7$ (average value 0.015). This would indicate a weaker Li−O bond in $Li_2B_4O_7$ in contrast to the calculated defect formation energies. But in $Li_2B_4O_7$ the overlap population decays very slowly. Second-nearest O and B atoms still have overlap populations of 0.011 with the Li atom. This indicates a more covalent nature of the bond in $Li_2B_4O_7$ which can explain the larger $E_{de}(V)$. In Li_2O all overlap populations are zero except for the nearest neighbors.

The relaxation energies E_R, 0.8 eV with PW1PW and 0.4 eV with PW91-PAW, obtained for LTB are in the order of 6−10% of the defect formation energies. The absolute values of E_R are in the same range as obtained for Li_2O.[34]

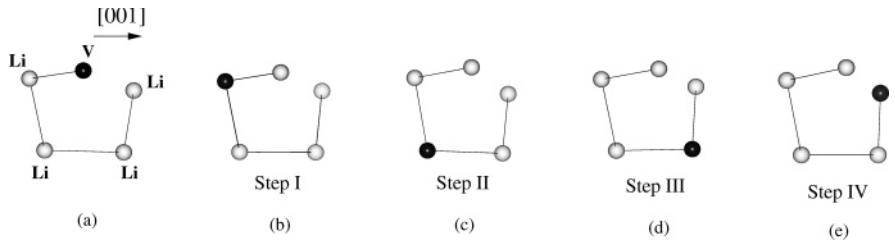

Figure 4. Schematic representation of the Li^+ ion migration in LTB (top view).

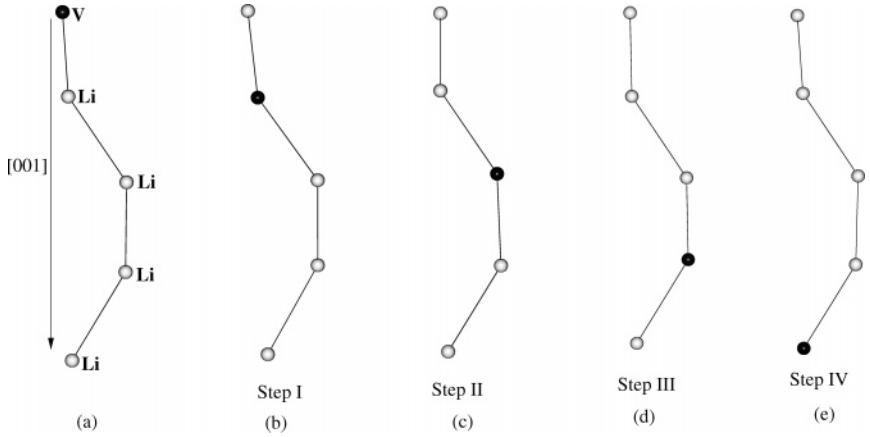

Figure 5. Schematic representation of the Li^+ ion migration in LTB (side view).

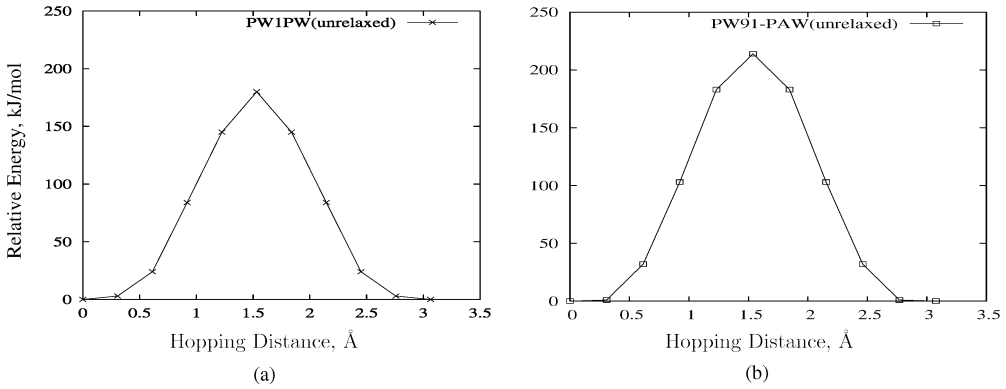

Figure 6. Potential energy curves for Li^+ ion migration in LTB without relaxation: (a) PW1PW and (b) PW91-PAW.

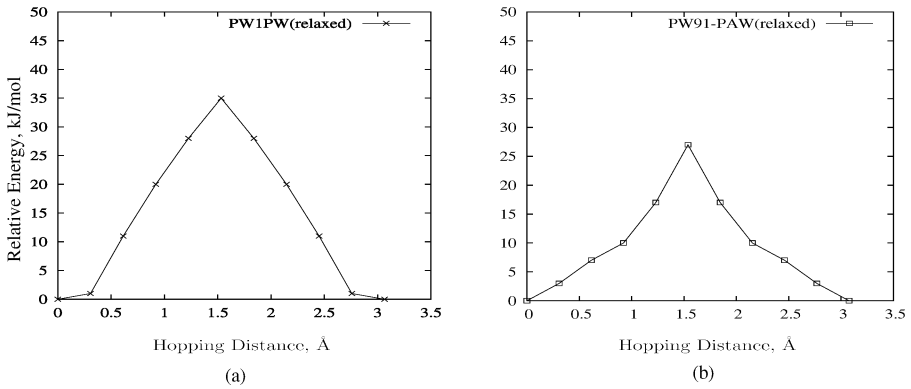

Figure 7. Potential energy curves for Li^+ ion migration in LTB with relaxation: (a) PW1PW and (b) PW91-PAW.

The effect of relaxation is further investigated by measuring the changes of distances of the nearest oxygen atoms, boron atoms, and lithium atoms with respect to the defect position during geometry optimization. In nondefective LTB, the Li atom is surrounded by four oxygen atoms in a distorted tetrahedral arrangement.[17,19] The four lithium−oxygen distances range from 1.97 to 2.17 Å.[17] Thereupon follows a fifth lithium−oxygen distance of 2.61 Å, forming a oxygen five-vertex polyhedron.[17,23] The next lithium−oxygen distances are 2.85 Å and more. In the following the six nearest oxygen atoms are considered to show the effect of relaxation (Figure 1). In Table 3, the calculated distances of O atoms from the vacancy before and after relaxation are shown. Here r_1 to r_6 denote the distances of O1−O6 from the vacancy. The numbering follows that in Figure 1. With both methods an increase of the oxygen-defect position distance is obtained. This is due to the fact that the electrostatic attraction by the Li^+ ion is missing. The removal of a neutral Li atom creates a hole in the valence band. One of the surrounding oxygen atoms which was formally O^{2-} in stoichiometric LTB becomes O^-. One unpaired electron is localized on the 2p orbital of one of those oxygen atoms. It should be noted that the sixth oxygen atom shows a small relaxation, +0.2% (PW1PW) and +0.4% (PW91-PAW), indicating that relaxation is mainly restricted to the nearest neighbors of the vacancy.

The calculated distances of the three nearest boron atoms and two nearest lithium atoms from the vacancy before and after optimization are shown in Table 4. r_1, r_2, and r_3 denote the distance of three boron atoms, respectively, and r_4 denotes the distance of two lithium atoms from the vacancy. Two of the boron atoms move toward the vacancy, while the position of the third boron atom is unchanged with both methods, Δr = 0.0% (PW1PW) and −0.2% (PW91-PAW). Also the two nearest lithium atoms show an inward relaxation of −4.2% with the PW1PW and −2.9% with the PW91-PAW approach. This behavior can be explained by the reduced electrostatic repulsion

TABLE 5: Comparison of Calculated Activation Energies E_A (eV) with and without Relaxation with Experimental Values

method	PW1PW	PW91-PAW	exptl[25]
unrelaxed	1.87	2.22	
relaxed	0.37	0.27	0.42, 0.46

of the positively charged boron and lithium ions after removal of a Li. The movement of the nearest Li neighbors around the vacancy in LTB is in line with the corresponding geometry changes in $Li_{2-x}O$,[34] where the nearest Li atoms show strong inward relaxation.

The study of electronic properties is performed by calculating the density of states (DOS) of the defective supercells. The DOS for a defective $Li_{16}B_{32}O_{56}$ supercell obtained with PW1PW is shown in Figure 2. PW91-PAW shows qualitatively the same behavior. The main difference to PW1PW is that the energetic difference between occupied and unoccupied bands is smaller with PW91-PAW. The Li^+ vacancy introduces an extra unoccupied level 0.26 eV above the Fermi level E_F, which is marked by an arrow in Figure 2. With PW91-PAW this energy difference is virtually identical, 0.27 eV. This band is mainly composed of oxygen p orbitals from atoms surrounding the vacancy site. In the analysis of the electronic structure obtained with PW1PW, it is found that the p orbitals of one of the four nearest oxygen atoms have much larger contributions than those of the other atoms. This corresponds to the simplified picture of a change from O^{2-} to O^- for a single atom. With PW91-PAW, the contributions to the defect band are more evenly distributed; therefore the hole is less localized.

3.3. Migration of Li^+ Ion. In LTB, a Li^+ ion migrates through a one-dimensional channel of ion conduction path in the (001) direction.[23] In this channel, Li ions form five-vertex oxygen polyhedra (LiO_5). The high atomic packing density and the rigidity of triangular and tetrahedral boron−oxygen polyhedra prevent direct jumps of Li ions along the tetragonal axis.[23] It is assumed that the Li^+ ion migrates through the large triangular faces of the two nearest oxygen five-vertex polyhedra facing each other. In Figure 3, two nearest oxygen five-vertex polyhedra, one of a Li ion and the other of an adjacent Li vacancy (V), are shown. The arrow shows the direction of the migrating Li^+ ion toward the vacancy. Two schematic views of the Li^+ ion migration process in LTB are presented in Figures 4 and 5. The migrating Li^+ ion and the vacancy V are in their original positions in Figures 4a and 5a. The migration path is modeled in four steps. In step I (Figures 4b and 5b), one Li^+ ion migrates to the adjacent vacancy. The migrating Li^+ ion accesses to the position of the vacancy, and the vacancy is created at the original position of the migrating ion. Similarly, in steps II−IV (Figures 4c, 4d, and 4e or 5c, 5d, and 5e), the Li^+ ion migrates along the (001) direction.

The calculated values of the Li hopping distance are 3.06 and 3.08 Å, with PW1PW and PW91-PAW, respectively, in good agreement with the experimental hopping distance of 3 Å.[23] In Figure 6, the potential energy curves for the Li^+ ion migration in LTB for unrelaxed systems are shown. In each step, the migration path is modeled in 10 substeps. The central substep was considered as an approximation of the corresponding transition structure. The activation energy E_A was calculated (for both the unrelaxed and relaxed systems) as the energy difference of the approximate transition structure and the initial structure where the vacancy is on a regular site. In Table 5, the calculated activation energies are compared with the experimental values.[25] For every step E_A is the same reflecting that the local environments of the migrating Li^+ ion and the vacancy are identical. Therefore, only one step is shown in the figure. For the unrelaxed system, both PW1PW and PW91-PAW methods give values that are too large (1.87 and 2.22 eV, respectively) for E_A compared to the experiment (0.42−0.46 eV, Table 5). This is in line with the previous finding for the Li^+ ion diffusion in Li_2O[34] and demonstrates the high importance of local relaxation for the calculation of activation barriers. The potential energy curves for Li^+ ion migration for the fully relaxed systems are shown in Figure 7. Both methods PW1PW (0.37 eV) and PW91-PAW (0.27 eV) now give good agreement with the experimental activation energies. As for Li_2O,[34] the PW1PW value better agrees with the experimental activation energy for LTB, deviating by only 0.05 eV.

4. Summary and Conclusions

The formation energy of a Li vacancy, the effect of structural relaxation around the Li vacancy, and the effect of the vacancy defect on the electronic properties of LTB crystal were investigated with two density-functional methods PW1PW and PW91-PAW. With both methods defect formation energies around 7 eV are obtained. Local relaxation has a moderate effect on the formation energy. Significant structural changes are only observed for the first shell of oxygen atoms and the closest boron and lithium atoms surrounding the Li vacancy site. The Li defect introduces an unoccupied level mainly composed of oxygen 2p orbitals slightly above the top of the valence band.

The Li^+ ion migration through a one-dimensional channel of five-vertex oxygen polyhedra along the tetragonal axis of LTB crystal was studied. The calculated activation energies for this process (0.37 eV with PW1PW and 0.27 eV with PW91-PAW) are in good agreement with measured values from the literature. Local relaxation has a much larger impact on the calculated activation energy for Li migration than for the formation of the Li vacancy defect itself. The presented methods and models have demonstrated that they provide sufficient accuracy for the description of bulk and defect properties for complex systems as $Li_2B_4O_7$. This experience provides the basis for future studies of even more complex systems such as interfaces between Li_2O and B_2O_3.

Acknowledgment. This work was supported the State of Lower Saxony, Germany, by a "Georg Christoph Lichtenberg" fellowship (M. M. Islam).

References and Notes

(1) Kosinski, J. A.; Lu, Y.; Ballato, A. *IEEE Trans. Ultrason., Ferroelectrics, Freq. Control* **1994**, *41*, 473.

(2) Komatsu, R.; Sugawara, T.; Watanabe, N. *Rev. Laser Eng.* **1999**, *27*, 541.

(3) Hee-Rak, J.; Byung-Moon, J.; Jung-Won, Ch.; Jung-Nam, K. *Mater. Lett.* **1997**, *30*, 41.

(4) Otsuka, K.; Funami, M.; Ito, M.; Katsuda, H.; Tacano, M.; Adachi, M.; Kawabata, A. *Jpn. J. Appl. Phys.* **1995**, *34*, 2646.

(5) Takeuchi, M.; Odagawa, I.; Tanaka, M.; Yamanouchi, K. *Jpn. J. Appl. Phys.* **1997**, *36*, 3091.

(6) Shestopalov, K. V.; Nefedov, V. A.; Zadneprovsky, B. I. *IEEE Int. Freq. Control Symp., Proc.* **1994**, 301.

(7) Whatmore, R. W.; Shorrocks, N. M.; O'Hara, C.; Ainger, F. W.; Young, I. M. *Electron. Lett.* **1981**, *17*, 11.

(8) Komatsu, R.; Sugawara, T.; Sassa, K.; Sarukura, N.; Liu, Z.; Izumida, S.; Segawa, Y.; Uda, S.; Fukuda, T.; Yamanouchi, K. *Appl. Phys. Lett.* **1997**, *70*, 3492.

(9) Sugawara, T.; Komatsu, R.; Uda, S. *Solid State Commun.* **1998**, *107*, 233.

(10) Adachi, M.; Nakazawa, K.; Kawabata, A. *Ferroelectrics* **1997**, *195*, 123.

(11) Filipiak, J.; Majchrowski, A.; Lukasiewicz, T. *Arch. Acoust.* **1994**, *19*, 131.

(12) Bhalla, A. S.; Cross, L. E.; Whatmore, R. W. *Jpn. J. Appl. Phys.* **1985**, *24*, 727.
(13) Ono, M.; Sakai, M.; Fujiwara, Y.; Wakatsuki, N. *IEEE Ultrason. Symp., Proc.* **1997**, 1047.
(14) Furetta, C.; Weng, P. S. *Operation Thermoluminescent dosimetry*; World scientific: London, 1998.
(15) Mahesh, K.; Weng, P. S.; Furetta, C. *Thermoluminescence in solids and its applications*; Nuclear Technology Publishing: Ashford, 1989.
(16) Dolzhenkova, E. F.; Baumer, V. N.; Tolmachev, A. V.; Hunda, B. M.; Puga, P. P. *Int. Conf. Inorg. Scintillators and Their Applications, 6th* **2001**, 210.
(17) Radaev, S. F.; Muradyan, L. A.; Malakhova, L. F.; Ya. Burak, V.; Simonov, V. I. *Kristallografiya* **1989**, *34*, 1400.
(18) Krogh-Moe, J. *Acta Crystallogr.* **1962**, *15*, 190.
(19) Krogh-Moe, J. *Acta Crystallogr., B* **1968**, *24*, 179.
(20) Hanbin, L.; Guangqiu, S.; Xiaoqing, W.; Jingzhi, W.; Denzhong, S. *Prog. Cryst. Growth Character.* **2000**, *40*, 235.
(21) Aliev, A. É.; Burak, Ya. V.; Lyseiko, I. T. *Izv. Akad. Nauk SSSR, Neorg. Mater.* **1990**, *26*, 1991.
(22) Burak, A. V.; Lyseiko, I. T.; Garapin, I. V. *Ukr. Fiz. Zh.* **1989**, *34*, 226.
(23) Rizak, I. M.; Rizak, V. M.; Baisa, N. D.; Bilanich, V. S.; Boguslavskiĭ, M. V.; S. Stefanovich, Yu.; Golovei, V. M. *Cryst. Rep.* **2003**, *48*, 676.
(24) Kim, C.-S.; Park, J.-H.; Moon, B. K.; Seo, H.-J.; Choi, B.-Ch.; Hwang, Y.-H.; Kim, H. K.; Kim, J. N. *J. Appl. Phys.* **2003**, *94*, 7246.
(25) Kim, C.-S.; Kim, D. J.; Hwang, Y.-H.; Kim, H. K.; Kim, J. N. *J. Appl. Phys.* **2002**, *92*, 4644.
(26) Rizak, V. M.; Rizak, I. M.; Bausa, N. D.; Bilanych, V. S.; Stefanovych, S. Yu.; Bohuslavskii, M. B.; Holovey, V. M. *Ferroelectrics* **2003**, *286*, 771.
(27) Kim, C.-S.; Hwang, Y. H.; Kim, H. K.; Kim, J. N. *Phys. Chem. Glass.* **2003**, *44*, 166.
(28) Button, D. P.; Mason, L. S.; Tuller, H. L.; Uhlmann, D. R. *Solid State Ionics* **1983**, *9/10*, 585.
(29) Bredow, T.; Gerson, A. R. *Phys. Rev. B* **2000**, *61*, 5194.
(30) Perdew, J. P.; Wang, Y. *Phys. Rev. B* **1992**, *45*, 13244.
(31) Perdew, J. P.; Chevary, J. A.; Vosko, S. H.; Jackson, K. A.; Penderson, M. R.; Singh, D. J.; Fiolhais, C. *Phys. Rev. B* **1992**, *46*, 6671.
(32) Adamo, C.; Barone, V. J. *Chem. Phys.* **1998**, *108*, 664.
(33) Gerson, A. R.; Bredow, T.; Pacchioni, G.; Simpson, D. J.; Jones, R. *Ionics* **2001**, *7*, 290.
(34) Islam, M. M.; Bredow, T.; Minot, C. *J. Phys. Chem. B* **2006**, *110*, 9413.
(35) Islam, M. M.; Bredow, T.; Minot, C. *Chem. Phys. Lett.* **2006**, *418*, 565.
(36) Islam, M. M.; Maslyuk, V. V.; Bredow, T.; Minot, C. *J. Phys. Chem. B* **2005**, *109*, 13597.
(37) Maslyuk, V. V.; Islam, M. M.; Bredow, T. *Phys. Rev. B* **2005**, *72*, 125101.
(38) Saunders, V. R.; Dovesi, R.; Roetti, C.; Orlando, R.; Zicovich-Wilson, C. M.; Harrison, N. M.; Doll, K.; Civalleri, B.; Bush, I.; D'Arco, Ph.; Llunell, M. *CRYSTAL2003 User's Manual*, University of Torino, Torino, 2003.
(39) Ojamäe, L.; Hermansson, K.; Pisani, C.; Causà, M.; Roetti, C. *Acta Crystallogr., B* **1994**, *50*, 268.
(40) Orlando, R.; Dovesi, R.; Roetti, C. *J. Phys.: Condens. Matter.* **1990**, *2*, 7769.
(41) Catti, M.; Valerio, G.; Dovesi, R.; Causà, M. *Phys. Rev. B* **1994**, *49*, 14179.
(42) Kresse, G.; Hafner, J. *Phys. Rev. B* **1993**, *47*, 558.
(43) Kresse, G.; Hafner, J. *Phys. Rev. B* **1993**, *48*, 13115.
(44) Kresse, G.; Hafner, J. *Phys. Rev. B* **1994**, *49*, 14251.
(45) Kresse, G.; Joubert, J. *Phys. Rev. B* **1999**, *59*, 1758.
(46) Blöchl, P. E. *Phys. Rev. B* **1994**, *50*, 17953.
(47) Kubaschewski, O.; Alock, C. B.; Spencer, P. J. *Materials Thermochemistry*, 6th ed.; Pergamon Press: New York, 1992; p 288.
(48) Ogorodnikov, I. N.; Pustovarov, V. A.; Kurzhalov, A. V.; Isaenko, L. I.; Kirm, M.; Zimmerer, G. *Phys. Solid State* **2000**, *42*, 464.